

## Quantitative electrochemical control over optical gain in colloidal quantum-dot and quantum-well solids

Geuchies, Jaco J.; Brynjarsson, Baldur; Grimaldi, Gianluca; Du Fossé, Indy; Dijkhuizen, Robbert; Koel, Marijn; Gudjonsdottir, Solrun; Van Der Stam, Ward; Evers, Wiel H.; Geiregat, Pieter

**DOI**

[10.1117/12.2569413](https://doi.org/10.1117/12.2569413)

**Publication date**

2020

**Document Version**

Final published version

**Published in**

Proceedings of SPIE

**Citation (APA)**

Geuchies, J. J., Brynjarsson, B., Grimaldi, G., Du Fossé, I., Dijkhuizen, R., Koel, M., Gudjonsdottir, S., Van Der Stam, W., Evers, W. H., Geiregat, P., Houtepen, A. J., & More Authors (2020). Quantitative electrochemical control over optical gain in colloidal quantum-dot and quantum-well solids. In C. Nielsen, D. Congreve, & A. J. Musser (Eds.), *Proceedings of SPIE: Physical Chemistry of Semiconductor Materials and Interfaces XIX* (Vol. 11464). Article 114640R (Proceedings of SPIE - The International Society for Optical Engineering; Vol. 11464). SPIE. <https://doi.org/10.1117/12.2569413>

**Important note**

To cite this publication, please use the final published version (if applicable).  
Please check the document version above.

**Copyright**

Other than for strictly personal use, it is not permitted to download, forward or distribute the text or part of it, without the consent of the author(s) and/or copyright holder(s), unless the work is under an open content license such as Creative Commons.

**Takedown policy**

Please contact us and provide details if you believe this document breaches copyrights.  
We will remove access to the work immediately and investigate your claim.

# PROCEEDINGS OF SPIE

[SPIDigitalLibrary.org/conference-proceedings-of-spie](https://spiedigitallibrary.org/conference-proceedings-of-spie)

## Quantitative electrochemical control over optical gain in colloidal quantum-dot and quantum-well solids

Geuchies, Jaco, Brynjarsson, Baldur, Grimaldi, Gianluca, Du Fossé, Indy, Dijkhuizen, Robbert, et al.

Jaco J. Geuchies, Baldur Brynjarsson, Gianluca Grimaldi, Indy Du Fossé, Robbert Dijkhuizen, Marijn Koel, Solrun Gudjonsdottir, Ward van der Stam, Wiel H. Evers, Pieter Geiregat, Zeger Hens, Arjan J. Houtepen, "Quantitative electrochemical control over optical gain in colloidal quantum-dot and quantum-well solids," Proc. SPIE 11464, Physical Chemistry of Semiconductor Materials and Interfaces XIX, 114640R (20 August 2020); doi: 10.1117/12.2569413

**SPIE.**

Event: SPIE Nanoscience + Engineering, 2020, Online Only

# Quantitative electrochemical control over optical gain in colloidal quantum-dot and quantum-well solids

Jaco J. Geuchies<sup>†</sup>, Baldur Brynjarsson<sup>†</sup>, Gianluca Grimaldi<sup>†\*</sup>, Indy Du Fossé<sup>†</sup>, Robbert Dijkhuizen<sup>†</sup>, Marijn Koel<sup>†</sup>, Solrun Gudjonsdottir<sup>†</sup>, Ward van der Stam<sup>†§</sup>, Wiel H. Evers<sup>†</sup>, Pieter Geiregat<sup>§</sup>, Zeger Hens<sup>§</sup>, Arjan J. Houtepen<sup>†</sup>

<sup>†</sup> Optoelectronic Materials Section, Faculty of Applied Sciences, Delft University of Technology, Van der Maasweg 9, 2629 HAZ Delft, The Netherlands.

<sup>§</sup> Physics and Chemistry of Nanostructures Group (PCN), Ghent University, B-9000 Ghent, Belgium

\* Current address: Center for Nanophotonics, AMOLF, Science Park 104, 1098 XG Amsterdam, The Netherlands.

<sup>§</sup> Current address: Inorganic Chemistry and Catalysis, Debye Institute for Nanomaterials Science, Utrecht University, Universiteitsweg 99, 3584 CG Utrecht, The Netherlands.

## ABSTRACT

Solution processed quantum dot (QD) lasers are one of the holy-grails of nanoscience. They are not yet commercialized because the lasing threshold is too high: one needs  $> 1$  exciton per QD, which is hard to achieve due to fast non-radiative Auger recombination. The threshold can however be reduced by electronic doping of the QDs, which decreases the absorption near the band-edge, such that the stimulated emission (SE) can easily outcompete absorption. Here, we show that by electrochemically doping films of CdSe/CdS/ZnS QDs we achieve quantitative control over the gain threshold. We obtain stable and reversible doping more than two electrons per QD. We quantify the gain threshold and the charge carrier dynamics using ultrafast spectroelectrochemistry and achieve quantitative agreement between experiments and theory, including a vanishingly low gain threshold for doubly doped QDs. Over a range of wavelengths with appreciable gain coefficients, the gain thresholds reach record-low values of  $\sim 10^{-5}$  excitons per QD. These results demonstrate an unprecedented level of control over the gain threshold in doped QD solids, paving the way for the creation of cheap, solution-processable low-threshold QD-lasers.

## INTRODUCTION

Colloidal semiconductor quantum dots (QDs) are attractive materials for solution-processable and color-tunable lasers<sup>1-4</sup>. Additionally, having discrete electronic states with finite degeneracy, QDs are ideal systems to achieve low threshold optical gain, promising a reduction of the threshold current in lasers. However, the larger-than-unity degeneracy of the conduction and valence-band levels implies that multiexcitons are required to achieve population inversion in QDs, i.e. for stimulated emission (SE) to outcompete absorption. Since Auger recombination is efficient in QDs<sup>5</sup>, multiexcitons have short lifetimes, typically  $< 100\text{ps}$ , implying that it is difficult to achieve/maintain a population sufficient for gain. Additionally, ultrafast charge-carrier trapping can compete with the build-up of optical gain when the trapping rates are similar to the time for the QDs to achieve population inversion<sup>6</sup>.

A controllable method to suppress absorption employs QD charging<sup>7-9</sup>. In 2004, pioneering work on electrochemical charging by the group of Guyot-Sionnest showed a reduction in the threshold for amplified stimulated emission (ASE)<sup>10</sup>. Recently, Wu et al. demonstrated nearly thresholdless optical gain using photochemical doping as a strategy to charge the QDs<sup>11</sup>, which, when coupled to a distributed feedback grating, shows sub-single exciton lasing.<sup>12</sup> While these recent results show the promise of QD charging for lasing, there is limited and only temporary control over the charge density and as a result, thresholdless gain has not been achieved. Electrochemical doping has the advantage that the electrochemical potential can be fixed and held constant over a QD film. When the QDs are sufficiently passivated with stable shells, this results in a stable and homogeneous doping density of the QD film.<sup>13,14</sup>

## RESULTS AND DISCUSSION

We synthesized wurtzite core-shell-shell CdSe/CdS/ZnS QDs for the experiments presented here. Details regarding the synthesis can be found in references<sup>15–17</sup>. The steady-state absorption and photoluminescence (PL) spectra, and a representative transmission electron microscopy image are shown in Figure 1(a). The epitaxial shells increase the absorption cross-section of the QDs at the excitation wavelength, boost the electrochemical stability of the QDs<sup>13</sup> and lead to a PL quantum yield of 81% in solution.

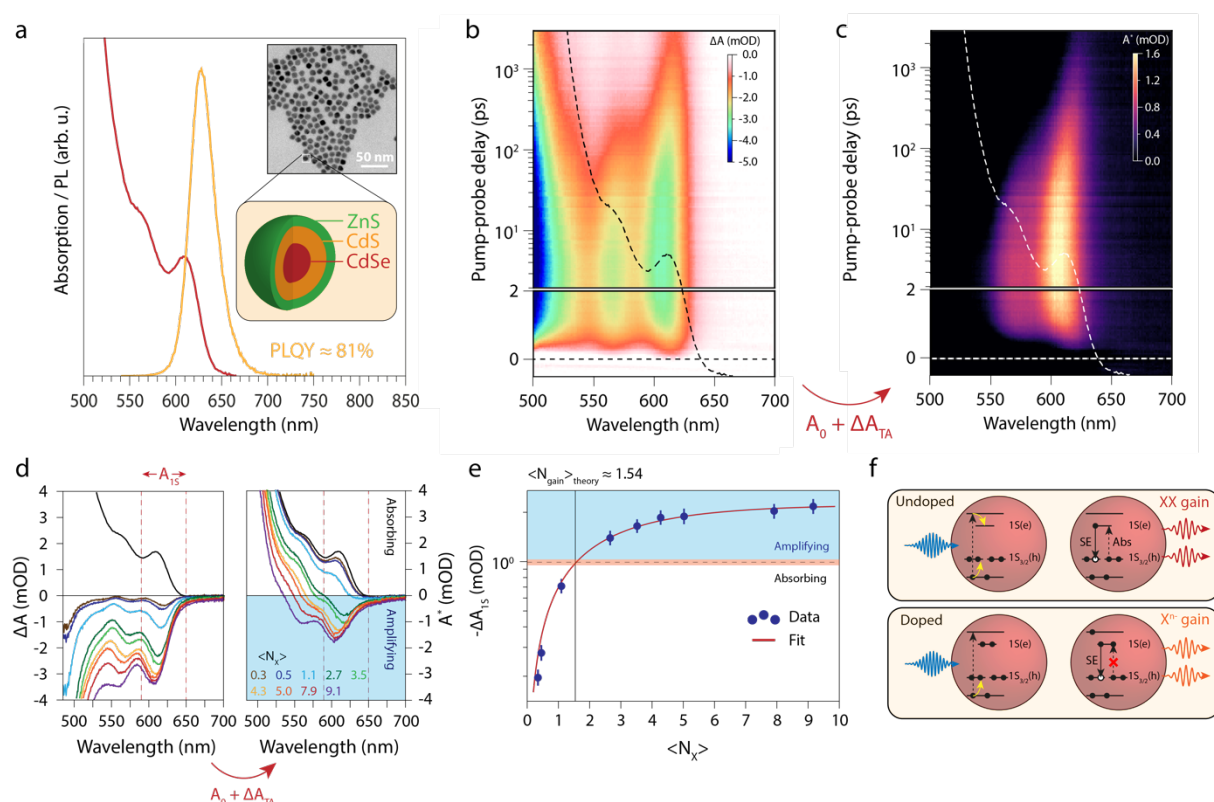


**Figure 1: Benchmarking the neutral CdSe/CdS/ZnS QDs in solution. (a)** Steady-state absorption and PL spectra of the CdSe/CdS/ZnS QDs used throughout this work. The insets show a TEM micrograph of the QDs, which have a diameter of  $10.9 \pm 1.0$  nm, and a schematic of the QDs. **(b)** 2D TA image for a pump wavelength of 400 nm and excitation density of  $\langle N_X \rangle = 7.9$ . The black dotted line shows the steady-state absorption spectrum. **(c)** Time-dependent excited state absorption spectrum (or gain-map), obtained from **(b)**, where all the positive absorption is colored black, and the negative absorption (gain) is colored following the scale

bar. **(d)** Spectral slices at a pump-probe delay time of 5 ps for increasing pump-fluence. The left image displays the differential absorption spectra, whereas the right image shows the excited-state absorption spectra. **(e)** Quantification of the optical gain threshold in solution, showing  $-\Delta A$  (@ 5ps pump-probe delay time) versus  $\langle N_X \rangle$ . The red line indicates a heuristic fit (increasing exponential function) to the data, used to determine the gain threshold. **(f)** Schematic of the mechanism for low threshold optical gain in undoped and doped QDs. Upon above-bandgap-excitation, both the electron and hole will cool down to the band-edges. In the n-doped QDs, the 1S absorption transition is already blocked. Hence, stimulated emission does not have to compensate for the absorption process, which leads to zero-threshold optical gain.

To benchmark these QDs we first measure the optical gain threshold in solution. We determine the absorption cross section ( $\sigma = 3.6 \pm 0.2 \cdot 10^{-14} \text{ cm}^2$  at the 400 nm pump wavelength) of the QDs, from the fluence dependence of Auger recombination<sup>6,18</sup>. Using the measured photon fluence  $J$ , we determine the average number of photogenerated excitons per QD,  $\langle N_X \rangle = J\sigma$ . Figure 1(b) shows a colormap of a TA measurement on the QDs. By adding the steady-state absorption,  $A_0$ , to the transient absorption, we obtain a gain map, as shown in Figure 1(c), showing in color the region of the spectrum characterized by negative absorption in the excited state, i.e. optical gain. To quantify the gain spectra and gain threshold, we take spectral slices at 5 ps, after thermalization of hot carriers, which is shown in Figure 1(d). The gain of the lowest the energy transition ((1S(e) – 1S<sub>3/2</sub>(h), the 1S transition) starts redshifted compared to the steady-state absorption spectrum, but shows a distinct blueshift with increasing excitation fluence (to a maximum of 20 meV). This is in agreement with models by Bisschop et al.<sup>19</sup>, who showed that the biexciton binding energy becomes repulsive when thick CdS shells are grown around the QDs.

To quantitatively evaluate the optical gain, we spectrally average the TA spectrum over the band-edge transition at 5 ps time delay [dashed vertical lines in Fig 1(d)]. Comparing the averaged bleach, presented in Figure 1(e), with the average absorption over the same wavelength range (horizontal dashed line), we determined the 1S gain-threshold  $\langle N_{\text{gain},1\text{S}} \rangle$  to be  $1.55 \pm 0.07$  excitons per QD. This is in quantitative agreement with the theoretical value of  $\langle N_{\text{gain},1\text{S}} \rangle$  of 1.54 for a two-fold 1S(e) and four-fold 1S<sub>3/2</sub>(h) degeneracy, determined considering a Poissonian distribution of excitons over the QD<sup>20</sup>. Furthermore, we observe that the absorption of the 1S transition is completely inverted at 5 ps for the highest pump fluence ( $\langle N_x \rangle = 9.1$ ). At high pump fluences ( $\langle N_x \rangle \geq 3.5$ ), also the second transition (1S(e) – 2S<sub>3/2</sub>(h), the 2S transition) shows optical gain. These results show that the neutral QDs behave nearly ideally and their gain properties are understood quantitatively.

## ELECTROCHEMICAL DOPING OF QD FILMS

To quantify the relationship between optical gain and electronic doping, we need precise control over the doping density inside the QD film. Using spectroelectrochemical (SEC) measurements, we controllably inject carriers into the QD films, monitoring changes in the photoluminescence and absorption of the film to determine the doping density. We prepared QD-films by spincoating a QD dispersion in toluene on a conductive ITO-on-glass substrate, followed by crosslinking the QDs with 1,7-diaminoheptane, to ensure the films have a good electron mobility.

Figure 2(a) shows SEC differential absorption ( $\Delta A_{\text{SEC}}$ ) measurements. We sweep the potential between the open circuit potential (-0.30V vs. the Ag pseudoreference electrode (PRE), i.e. -0.77V vs. Fc/Fc<sup>+</sup>) and -1.50V (i.e. -1.97V vs. Fc/Fc<sup>+</sup>), while measuring the change in absorption of the QD film. Upon electron injection into the conduction band of the QD film, we observe a decrease of several absorption transitions as a result of state filling of the 1S(e) conduction band level. Figure 2(a) shows three electrochemical cycles, highlighting the excellent reversibility of  $\Delta A_{\text{SEC}}$ .  $\Delta A_{\text{SEC}}$ -spectra at selected potentials are shown in Figure 2(b). The magnitude of the band-edge bleach is equal to the ground state absorption ( $A_0$ ) at roughly -1.4V, indicating that the 1S(e) level is completely filled. Figure 2(c) shows the corresponding SEC photoluminescence spectra as a function of applied potential. The PL intensity drops severely upon electron injection into the conduction band, an expected consequence of increased Auger decay in the n-doped QDs<sup>13</sup>. Figure 2(d) shows PL spectra at different potentials.

Figure 2(e) shows the absorption spectra of the charged QD films, i.e. the sum of the  $\Delta A_{\text{SEC}}$  spectra and the ground state absorption spectrum. The 1S transition becomes transparent at -1.4V.

To quantify the charge density, we fitted a Gaussian to the 1S absorption bleach feature at every potential, as well as to the 1S feature in the ground state absorption spectrum. The average number of electrochemically injected electrons in the 1S(e) level is given by  $\langle n_{1S(e)} \rangle = 2 \cdot \Delta A_{1S(e)} / A_{0,1S(e)}$ , where we use the Gaussian amplitudes of the fitted 1S absorption and absorption bleach<sup>8</sup>. The resulting values of  $\langle n_{1S(e)} \rangle$  at each potential are shown, together with the normalized PL intensity, in Figure 2(f). Charging and discharging of the QD film is fully reversible, as the number of electrochemically injected electrons into the 1S(e) level oscillates between zero and two. Furthermore, we observe that the absorption bleach increases at the same potential as the PL starts to quench, a good indication of trap-free and electrochemically stable QDs<sup>13,21</sup>.

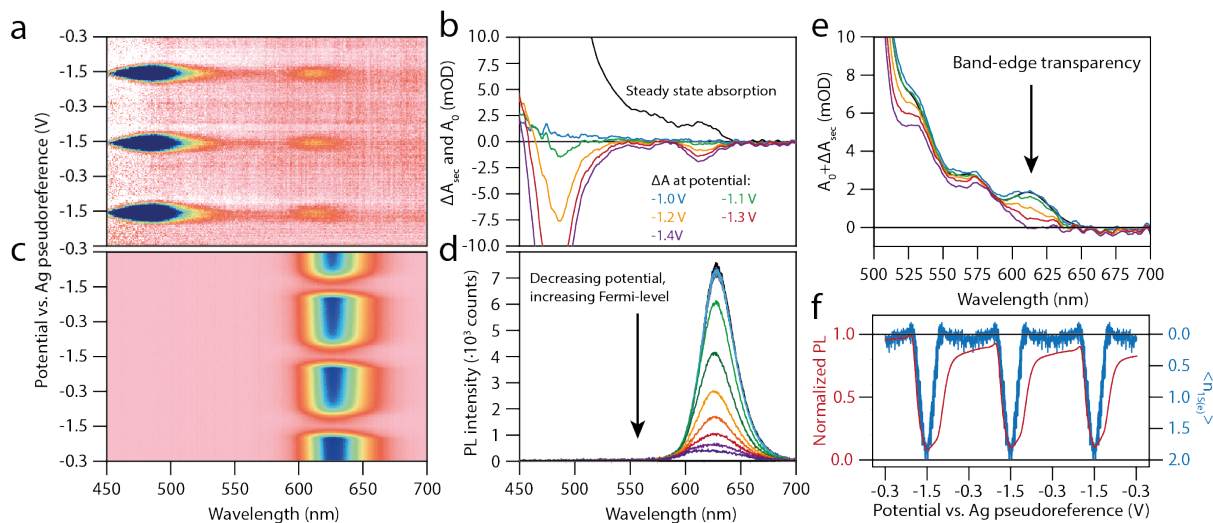


**Figure 2: Spectroelectrochemistry on a film of CdSe/CdS/ZnS QDs.** The potential during all SEC measurements was swept three times between the open circuit potential and -1.5V to check for sample stability. **(a)** SEC absorption measurements. Injection of electrons into the conduction band of the QDs is observed by bleaching of the band-edge (around 615 nm) and CdS shell (< 550 nm) transitions. **(b)**  $\Delta A_{\text{SEC}}$  spectra at different potentials. Charge injection

starts around -1.1V. Note that the band-edge bleach amplitude at the most negative potentials equals the amplitude of the absorption spectrum. (c) SEC PL measurements. As electrons are injected into the conduction band of the QDs, the PL quenches due to Auger recombination. (d) PL spectra at different potentials. The PL amplitude decreases due to enhanced Auger recombination. (e) Total absorption of the QD film, i.e.  $\Delta A_{\text{SEC}} + A_0$ . The band-edge transition becomes transparent at -1.4V. (f) Normalized PL and amplitude of the band-edge bleach as a function of applied potential. The drop in PL coincides with the injection of charges into the conduction band of the QDs, indicating a relatively trap-free QD film. The number of electrochemically injected  $1S(e)$  electrons oscillates between zero and two.

## ULTRAFAST SPECTROELECTROCHEMISTRY

To characterize the gain response of n-doped QD films, we performed fs transient absorption (fsTA) measurements while electrochemically controlling the doping density, which we refer to as ultrafast spectroelectrochemistry. The differential absorption signal,  $\Delta A_{\text{TA}}$ , can be added to the steady-state absorption spectrum of the sample to obtain the excited state absorption. The gain threshold is defined as the first excitation fluence resulting in a negative excited state absorption.

Figure 3 presents excited state absorption spectra for 400 nm excitation as a function of pump-probe delay time for various electrochemical doping densities ranging from  $\langle n_{1S(e)} \rangle = 0$  to 2 and excitation fluences ranging from  $\langle N_x \rangle = 0$  to 6.6. As optical excitation of a thin film of

semiconductor material results in changes in both the absorption and reflection of the film, all TA spectra are corrected for changes in reflectivity of the sample after photoexcitation<sup>22</sup>.

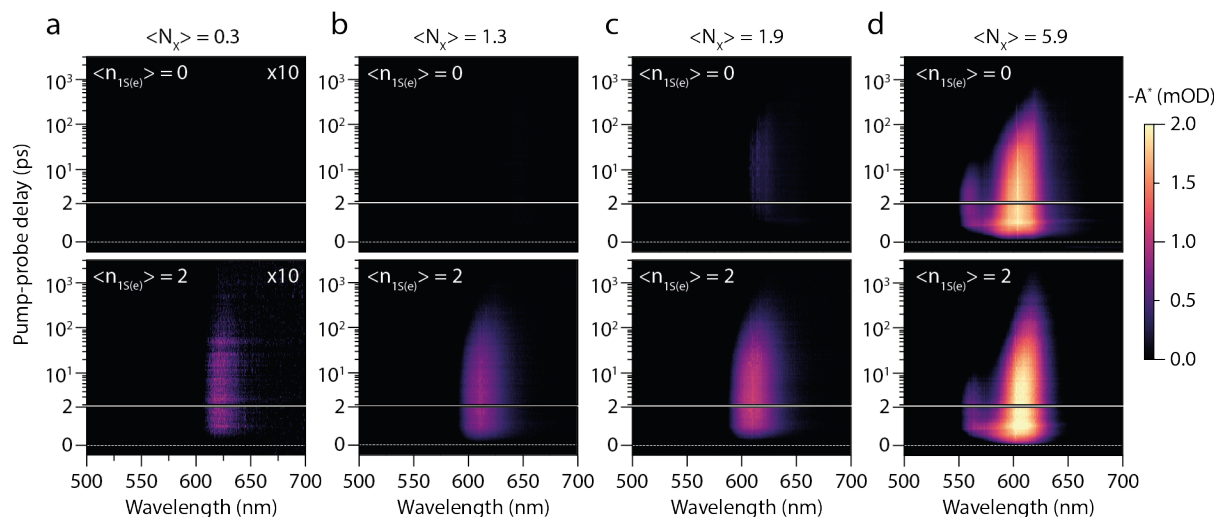


**Figure 3: Reduced threshold optical gain upon doping the QD solid with two electrons**

**per QD.** Excited state absorption maps (excitation at 400 nm) as a function wavelength and pump-probe delay time. The upper panels show absorbance of the undoped QD solid ( $\langle n_{1S(e)} \rangle = 0$ ), whereas the bottom panels show the doped QD solid ( $\langle n_{1S(e)} \rangle \sim 2$ ). (a) The low fluence data ( $\langle N_x \rangle = 0.3$ ) were multiplied by 10 for clarity. The doped QD solid already shows optical gain around 620 nm at the lowest excitation fluence. (b) For  $\langle N_x \rangle = 1.3$ , slightly below the theoretical threshold of  $\langle N_{\text{gain}} \rangle = 1.54$  for the undoped QDs, no signature of optical gain is observed in the undoped QDs, whereas the gain amplitude is increased for the doped solid. (c) For  $\langle N_x \rangle = 1.9$  a small amount of optical gain for the undoped QDs is observed. (d) For high photoexcitation density, resulting in  $\langle N_x \rangle = 5.9$ , both the undoped and doped QD solid show full inversion of the 1S transition, and a shorter-lived gain signal originating from the 2S transition.

The top row of Figure 3 shows gain maps for the undoped film, i.e.  $\langle n_{1S(e)} \rangle = 0$  (-0.3V vs Ag. PRE), whereas the bottom row shows gain maps are for  $\langle n_{1S(e)} \rangle = 2$  (at -1.5V vs. Ag PRE). From left to right the excitation density increases. Figure 3(a) shows the excited state absorption map for  $\langle N_x \rangle = 0.3$ . For clarity, the signal amplitude is multiplied by 10. For the

undoped QD film we do not observe any optical gain over the measured spectral window. Upon increasing the excitation fluence to  $\langle N_x \rangle = 1.9$ , we start to observe gain from the 1S transition in Figure 3(c). At the highest fluence presented here,  $\langle N_x \rangle = 5.9$ , we also observe optical gain from the 2S transition. In stark contrast, at a doping density of  $\langle n_{1S(e)} \rangle = 2$ , we observe light amplification of the 1S transition even for the lowest excitation fluence, as shown in the bottom panel of Figure 3(a). Upon increasing the fluence, the optical gain amplitude increases, and we again observe optical gain from the 2S transition at  $\langle N_x \rangle = 5.9$ . The data qualitatively show that electrochemical doping can drastically reduce the optical gain threshold. In the remainder of the manuscript we will quantify the relationship between optical gain, density of electrochemically injected carriers and density of excitons.

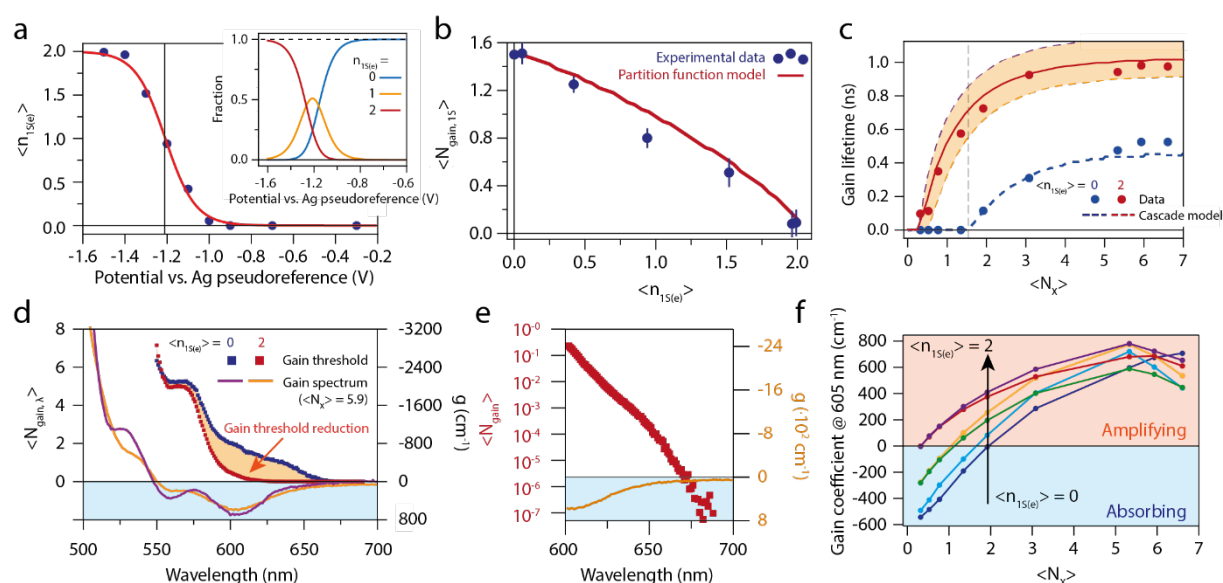


**Figure 4: Quantification and modelling of measured optical gain and determination of device-relevant parameters.** (a)  $\langle n_{1S(e)} \rangle$  versus the applied electrochemical potential. Blue datapoints represent the experimentally determined charge density, the red solid line is a Fermi-Dirac fit. The inset shows the distribution of neutral, singly-charged and doubly-charged QDs vs. applied potential as extracted from the fit. (b) Gain threshold  $\langle N_{\text{gain},1S} \rangle$  versus the average number of electrochemically injected electrons per QD  $\langle n_{1S(e)} \rangle$ . The blue datapoints represent the experimentally determined threshold, the solid red line is a model based on Poisson

statistics for photon excitation, Fermi-Dirac statistics for electron filling, and transition counting to estimate the absorption cross section of the band-edge transition. **(c)** Gain lifetimes as a function of  $\langle N_X \rangle$  for the neutral and doubly charged QD film. The blue and red dots are experimental data points, and the lines represent a model based on coupled rate-equations (with  $\langle n_{1S(e)} \rangle = 1.95, 1.9$  and  $1.85$  going from top to bottom). **(d)** Single wavelength gain threshold  $\langle N_{\text{gain},\lambda} \rangle$  vs. wavelength for the neutral and  $\langle n_{1S(e)} \rangle = 2$  doped QD film, shown as the blue and red squares respectively. For comparison, we also show the excited state absorption spectrum for the neutral and charged film for  $\langle N_X \rangle = 5.9$  (blue and red solid lines respectively), to demonstrate that the optical gain threshold vanishes at wavelengths where there is an appreciable gain coefficient. **(e)** a zoom-in of **(d)** the spectral region from 600-700 nm, plotted on a logarithmic scale. We observe  $\langle N_{\text{gain},\lambda} \rangle = 10^{-3}-10^{-5}$  in regions with significant negative absorption. **(f)** Gain coefficient at 605 nm for various doping densities. The gain coefficients saturate around  $800 \text{ cm}^{-1}$ .

Finally, we combine all experiments shown above to develop a model that quantitatively describes optical gain in doped QDs. We model the excited state absorption in a QD film using the transition model counting model discussed in ref<sup>6</sup>. As inputs we need to know the distribution of electrons and excitons over the QDs at each potential. First, fitting a Fermi-Dirac distribution for a two-fold degenerate level to  $\langle n_{1S(e)} \rangle$  as a function of the applied potential, shown in Figure 4(a), we obtain the fraction of neutral, singly charged and doubly charged QDs at each potential. Combined with a Poisson distribution of  $\langle N_X \rangle$  at each fluence this allows us to predict the gain threshold  $\langle N_{\text{gain},1S} \rangle$  as a function of  $\langle n_{1S(e)} \rangle$ . The modelled excited-state absorption is:

$$A_{\text{ensemble}}^*(\langle N_X \rangle, \langle n_{1S(e)} \rangle) = \sum_{n_{\text{chem}}=0}^2 \sum_{N=0}^{N_{\text{max}}} f(\langle n_{1S(e)} \rangle) \cdot P(\langle N_X \rangle, N) \cdot A^*(N, \langle n_{1S(e)} \rangle) \quad (1)$$

with  $P(\langle N_X \rangle, N)$  a Poisson distribution for the exciton density and  $f(\langle n_{1S(e)} \rangle)$  a Fermi-Dirac function describing electrochemical state-filling of the 1S(e) level (see SI, section S1). Equation 1 is numerically solved to determine the value  $\langle N_X \rangle$  where  $A^*_{\text{ensemble}} = 0$ . The prediction from this model is shown as the red solid line in Figure 4(b).

The data points in Figure 4(b) show the measured gain threshold  $\langle N_{\text{gain,1S}} \rangle$  as a function of  $\langle n_{1S(e)} \rangle$ , showing a decrease in threshold with increasing  $\langle n_{1S(e)} \rangle$ . Note that the red solid line is not a fit to the data, but a prediction based on independent experimental observables (i.e. the absorption cross section from fluence dependent Auger recombination data. The match between the experimental gain thresholds and the model prediction is excellent, demonstrating that we have quantitative control over the gain threshold, both experimentally and theoretically.

In Figure 4(c) we present the lifetime of the optical gain signal for the neutral QD film ( $\langle n_{1S(e)} \rangle = 0$ , blue datapoints), and the QD film with on average two electrons per QD (red datapoints). We define the optical gain lifetime as the amount of time after photoexcitation that the average excited state 1S absorption remains negative. The extracted gain lifetimes increase with both increasing  $\langle N_X \rangle$  and with increasing  $\langle n_{1S(e)} \rangle$ . For undoped QD films the highest gain lifetime is  $\sim 0.5$  ns, while for doped QD it reaches  $\sim 1$  ns. To model the gain dynamics, we set up a system of coupled differential equations that take Auger decay of (charged) multiexcitons into account. From the fluence-dependent fsTA data, we extract a biexciton lifetime of 310 ps. We assume that Auger rates scale with the number of electrons and holes as outlined by the group of Klimov<sup>5,23,24</sup>, which allows us to model the cascade of Auger processes controlling excitonic decay. As shown in Figure 4(c), we get good quantitative agreement with the experimental data.

These results demonstrate the possibility to use our analytical model to accurately describe the relationship between the carrier population and optical gain in QD solids. Furthermore, complementing the transition counting model with a description of excitonic decay allows a precise prediction of the gain lifetime. Having been validated on this dataset, the model provides useful insight on the lasing characteristics of different QD materials of known band-edge degeneracies and Auger lifetimes, and can be used to direct the development of novel devices.

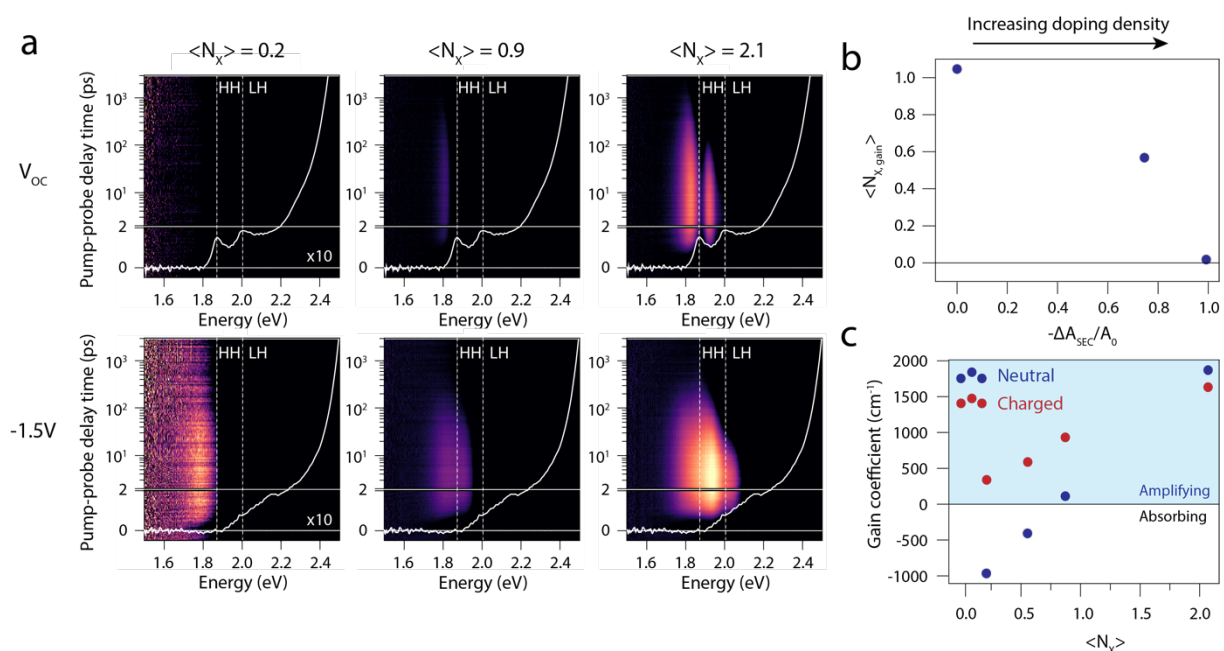
So far, we have focused on the spectrally averaged gain threshold  $\langle N_{\text{gain},1S} \rangle$ , as this is most insightful to study the effects of state filling on absorption and stimulated emission, without complications from spectral shifts that result from doping or optical excitation. However, for practical applications, a more relevant value is the gain threshold at a single wavelength, where light amplification is to take place,  $\langle N_{\text{gain},\lambda} \rangle$ . In Figure 4(d) we plot  $\langle N_{\text{gain},\lambda} \rangle$  as a function of wavelength for the undoped (blue squares) and the  $\langle n_{1S(e)} \rangle = 2$  charged (red squares) QD film. The decrease of the optical gain threshold is clearly visible for the 1S transition, highlighted with the yellow area in the graph. For comparison, the gain coefficient spectra (at a fluence of  $\langle N_X \rangle = 5.9$ ) are also plotted in the same figure. These are obtained from the excited state absorption spectra and the film thickness  $d = 116 \pm 13$  nm, as  $g = \frac{-A \cdot \ln(10)}{d}$ .

Figure 4(e) shows a zoom of Figure 4(d), but on a logarithmic scale. We observe that the threshold practically vanished for the doped film over a significant wavelength range. It becomes clear that, defined at a single wavelength, the gain threshold is somewhat arbitrary. In addition to a low threshold it is important that there is a significant gain coefficient at the amplified wavelength, at least large enough to compensate for losses that occur for the optical mode that is amplified. A typical loss coefficient in InGaAs/GaAs/AlGaAs laser diode arrays  $> 50 \text{ cm}^{-1}$ .<sup>25</sup> Taking this gain coefficient as the threshold for amplification we observe a record-

low single-wavelength thresholds of  $2.5 \cdot 10^{-5}$  excitons per QD, corresponding to a 400 nm pump fluence of 0.4 nJ/pulse/cm<sup>2</sup>.

Figure 4(f) shows the gain coefficient at 605 nm as a function of  $\langle N_x \rangle$  and for various doping densities. At a fixed value of  $\langle N_x \rangle$  the gain coefficient is always significantly higher for doped QD films than for the neutral film. The maximum gain coefficient for the doped QD film is  $\sim 800$  cm<sup>-1</sup>, which is similar to the intrinsic gain coefficient of colloidal QDs in solution and III-V epitaxial semiconductors ( $10^3$  cm<sup>-1</sup>).<sup>19,26</sup> This demonstrates the great promise of electrochemically doped QD films for use as low-threshold gain media with strong light amplification. The next step, currently underway in our lab, is to employ electrochemically doped QD films in devices such as DFB gratings<sup>12,27–30</sup>, micro-disk lasers<sup>31</sup>, and ring resonators<sup>32</sup>.

## ULTRAFAST SPECTROELECTROCHEMISTRY WITH NANOPATELET SOLIDS



**Figure 5: Optical gain in neutral and charged NPL solids. (a)** Excited-state absorption maps for different  $\langle N_x \rangle$  and doping densities (neutral top row, charged bottom row). Notice how the

maximum gain is achieved in between the HH and LH transition in the charged NPL film. **(b)** The optical gain threshold as a function of electrochemical fractional bleach (doping density). Data is spectrally integrated over the HH transition to account for spectral shifts. The gain threshold is reduced from  $\langle N_{x, \text{gain}} \rangle = 1.04$  to 0.02 excitons per NPL upon fully charging the NPL film. **(c)** Gain coefficients at 1.78 eV for the neutral NPL film and charged NPL film. To calculate the gain coefficients, we measured the film thickness to be 50.8 nm and assumed a volume fraction of NPLs of 0.5 in the film.

We perform similar experiments on solids consisting out of CdSe/CdS/ZnS core-shell-shell NPLs. These nanoplatelets seem to have higher absorption coefficients than QDs in solution due to the giant oscillator strength effect. This theoretically should also lead to higher gain coefficients. In Figure 5(a), we present the gain maps for a solid of these NPLs. As can be seen, we start to observe optical gain in the neutral NPL film around 1 exciton per platelet; a value that can be rationalized based on the splitting of the heavy-hole (HH) and light-hole (LH) bands in these quantum wells. Sharp, excitonic-like optical gain bands for both HH and LH bands are observed at higher fluences. When charging the NPL film, we observe broadband optical gain red shifted of the HH transition. At higher excitation fluences, the broadening increases, and compared to the neutral film, we only observe a broad gain band.

The spectrally integrated optical gain threshold is shown in Figure 5(b). Upon charging, we observe a decrease of the gain threshold from  $\langle N_x \rangle = 1$ , to  $\langle N_x \rangle = 0.02$  excitons per platelet, i.e. we effectively completely remove the optical gain threshold in the solid. Furthermore, when comparing the gain coefficients to those of QDs, we observe roughly three times higher magnitudes, which are not even in the saturation regime yet. These results demonstrate that both electrochemically charged QDs and NPLs are extremely viable candidates for solution-processed, low-threshold lasers.

## CONCLUSIONS

We have demonstrated precise experimental and theoretical control over the optical gain threshold in QD solids, via controlled and reversible electrochemical doping. After electrochemically injecting on average two electrons per QD into the 1S(e) electron level, we show that the spectrally integrated 1S gain threshold is as low as 0.09 excitons per QD. We achieve record low single wavelength gain thresholds down to  $\sim 10^{-5}$  excitons per QD, gain coefficients up to  $800 \text{ cm}^{-1}$ , and a gain lifetime of  $\sim 1 \text{ ns}$ . Furthermore, we are able to model the gain threshold reduction for the electrochemical charging and the resulting gain lifetimes quantitatively. Next to this, when using CdSe-based nanoplatelets (NPLs), we reach even lower spectrally integrated gain thresholds of 0.02 excitons/QD, and gain coefficients which go up to  $2000 \text{ cm}^{-1}$ , likely due to the giant oscillator strength effects in these colloidal quantum wells. These results pave the way to achieve optically pumped QD and NPL lasers operating at low excitation fluences.

## REFERENCES

1. Kovalenko, M. V. *et al.* Prospects of Nanoscience with Nanocrystals. *ACS Nano* **9**, 1012–1057 (2015).
2. Geiregat, P., Van Thourhout, D. & Hens, Z. A bright future for colloidal quantum dot lasers. *NPG Asia Mater.* **11**, 41 (2019).
3. Klimov, V. I. *et al.* Optical Gain and Stimulated Emission in Nanocrystal Quantum Dots. *Science (80-. )*. **290**, (2000).
4. Kagan, C. R. *et al.* Building devices from colloidal quantum dots. *Science* **353**, 545–610 (2016).
5. Klimov, V. I., Mikhailovsky, A. A., McBranch, D. W., Leatherdale, C. A. & Bawendi, M. G. Quantization of Multiparticle Auger Rates in Semiconductor Quantum Dots. *Science (80-. )*. **287**, 1011–1013 (2000).
6. Grimaldi, G. *et al.* Spectroscopic Evidence for the Contribution of Holes to the Bleach of Cd-Chalcogenide Quantum Dots. *Nano Lett.* **19**, 3002–3010 (2019).
7. Shim, M. & Guyot-Sionnest, P. n-type colloidal semiconductor nanocrystals. *Nature* **407**, 981–983 (2000).
8. Wang, C., Shim, M. & Guyot-Sionnest, P. Electrochromic Nanocrystal Quantum Dots. *Science (80-. )*. **291**, 2390–2392 (2001).
9. Yu, D., Wang, C. & Guyot-Sionnest, P. n-type conducting CdSe nanocrystal solids. *Science (80-. )*. **300**, 1277–1280 (2003).
10. Wang, C., Wehrenberg, B. L., Woo, C. Y. & Guyot-Sionnest, P. Light emission and amplification in charged CdSe quantum dots. *J. Phys. Chem. B* **108**, 9027–9031 (2004).
11. Wu, K., Park, Y.-S., Lim, J. & Klimov, V. I. Towards zero-threshold optical gain using charged semiconductor quantum dots. *Nat. Nanotechnol.* **12**, 1140–1147 (2017).
12. Kozlov, O. V. *et al.* Sub-single-exciton lasing using charged quantum dots coupled to a distributed feedback cavity. *Science (80-. )*. **365**, 672–675 (2019).
13. Van Der Stam, W. *et al.* Electrochemical modulation of the photophysics of surface-localized trap states in core/shell/(shell) quantum dot films. *Chem. Mater.* **31**, 8484–8493 (2019).
14. Vanmaekelbergh, D., Houtepen, A. J. & Kelly, J. J. Electrochemical gating: A method to tune and monitor the (opto)electronic properties of functional materials. *Electrochim. Acta* **53**, 1140–1149 (2007).
15. Hanifi, D. A. *et al.* Redefining near-unity luminescence in quantum dots with photothermal threshold quantum yield. *Science* **363**, 1199–1202 (2019).
16. Chen, O. *et al.* Compact high-quality CdSe–CdS core–shell nanocrystals with narrow emission linewidths and suppressed blinking. *Nat. Mater.* **12**, 445–451 (2013).
17. Boldt, K., Kirkwood, N., Beane, G. A. & Mulvaney, P. Synthesis of Highly Luminescent and Photo-Stable, Graded Shell CdSe/Cd<sub>x</sub>Zn<sub>1-x</sub>S Nanoparticles by In Situ Alloying. *Chem. Mater.* **25**, 4731–4738 (2013).
18. Makarov, N. S. *et al.* Spectral and Dynamical Properties of Single Excitons, Biexcitons, and Trions in Cesium–Lead-Halide Perovskite Quantum Dots. *Nano Lett.* **16**, 2349–2362 (2016).
19. Bisschop, S., Geiregat, P., Aubert, T. & Hens, Z. The Impact of Core/Shell Sizes on the Optical Gain Characteristics of CdSe/CdS Quantum Dots. *ACS Nano* **12**, 9011–9021 (2018).

20. Efros, A. L. *et al.* Band-edge exciton in quantum dots of semiconductors with a degenerate valence band: Dark and bright exciton states. *Phys. Rev. B - Condens. Matter Mater. Phys.* **54**, 4843–4856 (1996).
21. Jha, P. P. & Guyot-Sionnest, P. Photoluminescence switching of charged quantum dot films. *J. Phys. Chem. C* **111**, 15440–15445 (2007).
22. Ghosh, T., Aharon, S., Shpatz, A., Etgar, L. & Ruhman, S. Reflectivity Effects on Pump–Probe Spectra of Lead Halide Perovskites: Comparing Thin Films *versus* Nanocrystals. *ACS Nano* **12**, 5719–5725 (2018).
23. Klimov, V. I., McGuire, J. A., Schaller, R. D. & Rupasov, V. I. Scaling of multiexciton lifetimes in semiconductor nanocrystals. *Phys. Rev. B* **77**, 195324 (2008).
24. García-Santamaría, F. *et al.* Breakdown of volume scaling in auger recombination in CdSe/CdS heteronanocrystals: The role of the core-shell interface. *Nano Lett.* **11**, 687–693 (2011).
25. Kabanov, V. V. *et al.* Loss coefficient for amplified luminescence of laser diode arrays. *J. Appl. Spectrosc.* **77**, 810–816 (2011).
26. Pietryga, J. M. *et al.* Spectroscopic and Device Aspects of Nanocrystal Quantum Dots. *Chem. Rev.* **116**, 10513–10622 (2016).
27. Prins, F. *et al.* Direct Patterning of Colloidal Quantum-Dot Thin Films for Enhanced and Spectrally Selective Out-Coupling of Emission. *Nano Lett.* **17**, 1319–1325 (2017).
28. Chen, Y. *et al.* Flexible distributed-feedback colloidal quantum dot laser. *Appl. Phys. Lett.* **99**, 241103 (2011).
29. Roh, K. *et al.* Surface-emitting red, green, and blue colloidal quantum dot distributed feedback lasers. *Opt. Express* **22**, 18800 (2014).
30. Roh, J., Park, Y.-S., Lim, J. & Klimov, V. I. Optically pumped colloidal-quantum-dot lasing in LED-like devices with an integrated optical cavity. *Nat. Commun.* **11**, 271 (2020).
31. Zhu, Y. *et al.* On-Chip Single-Mode Distributed Feedback Colloidal Quantum Dot Laser under Nanosecond Pumping. *ACS Photonics* **4**, 2446–2452 (2017).
32. Le Feber, B., Prins, F., De Leo, E., Rabouw, F. T. & Norris, D. J. Colloidal-Quantum-Dot Ring Lasers with Active Color Control. *Nano Lett.* **18**, 1028–1034 (2018).